AUT Journal of Electrical Engineering

AUT J. Electr. Eng., 56(3) (2024) 361-376
DOI: 10.22060/eej.2024.22902.5569

Analysis and Design of a Novel Broadband and High-Efficiency Class-E/FJ Power Amplifier

Parastoo Rostami, Akram Sheikhi *

Department of Electrical Engineering, Lorestan University, Khorramabad, Iran

ABSTRACT: This paper presents a novel hybrid Class-E/FJ power amplifier (PA) that integrates Class-E/F PA and Class-J PA to formulate a high-efficiency as well as broadband performance. The theoretical relationships of the Class-E/F amplifier have been thoroughly examined, and the corresponding relationships and diagrams have been obtained. Furthermore, in the next step, theoretical analysis for Class-J has been derived, and the necessary conditions for achieving a strengthening relationship between Class-E/F and Class-J to achieve a hybrid Class-E/FJ PA have been investigated. Through the judicious configuration of parameter values, the proposed design achieves an efficiency range spanning from 61.2% to 73.4% across the 1.3-3.1 GHz. The paper delineates a systematic design process for a broadband Class-E/FJ PA based on derived theories. To validate the proposed approach, a meticulous design and fabrication process is undertaken for a 1.3-3.1 GHz broadband Class-E/FJ PA. Measurement results demonstrate that the PA can deliver a saturated output power ranging from 39.3 dBm to 42 dBm, accompanied by a gain within the 8-12 dB range. Additionally, the Power Added Efficiency (PAE) falls within the range of 58.9%-67% within the specified frequency band. A comparative analysis with similar predecessors reveals that the proposed PA outperforms others, exhibiting superior performance across a wide bandwidth.

Review History:

Received: Dec. 29, 2023
Revised: Apr. 17, 2024
Accepted: May, 28, 2024
Available Online: Jul. 01, 2024

Keywords:

Broadband
Class-E/F
Class-J
Class-E/FJ
Harmonic Control Circuit

1- Introduction

The PA finds extensive application in telecommunication systems. Transitioning towards broader bandwidth and heightened efficiency is a crucial necessity for enhancing the performance of contemporary wireless systems. Theoretically, various types of PAs, including Class-F [1, 2], Class-E [3], Class-F/E [4], and Class-E/F [5, 6], can achieve an efficiency of up to 100%. Regrettably, the bandwidth of these high-efficiency PAs is limited. To date, only a handful of studies have concentrated specifically on broadband Class-J PAs [7-11]. A high-efficiency quasi-Class-J power amplifier is presented in [7], that showcases a broadband output matching network (OMN) comprised of multi-stub microstrip lines. Notably, the amplifier incorporates a feature by utilizing negative second harmonic termination as a nonlinear output capacitor at saturation conditions. This implementation results in the generation of a harmonic drain current that opposes the transistor, inducing alterations in the waveform. In [8], the paper introduces a systematic design methodology for monolithic microwave integrated circuits (MMIC) Class-J PA. The methodology encompasses theoretical derivations taking into account the nonlinear drain-source resistance of transistors (R_{DS}). To validate the proposed approach, a 3.5–7 GHz, 0.5-W Class-J PA is implemented using a 0.1-μm AlGaAs–InGaAs pHEMT technology, that achieves 56% average PAE across the frequency band, while maintaining an average 11-dB small-signal gain. MMIC technology indeed involves a complex and intricate fabrication process. During the implementation phase, certain challenges and difficulties were encountered. The production of MMICs typically requires advanced semiconductor manufacturing techniques, where multiple active and passive components are integrated into a single chip. In [9], the letter investigates and refines the Class-J dynamic load modulation (DLM) PA, proposing a modified design methodology to broaden its bandwidth. Departing from conventional purely reactive load modulation approaches, the study emphasizes the manipulation of the resistive part of the load impedance to enhance the RF bandwidth. Experimental results show performance from 1.7 GHz to 2.3 GHz, achieving up to 50% PAE. A frequency-agile PA is introduced in [10]6, employing a modified Class-J theory. This innovative Class-J mode, referred to as clockwise-loaded Class-J (CLCJ), enables frequency-agile capabilities and enhanced efficiency when the drain supply voltage is designed with the fundamental and harmonic loads. The designed CLCJ PA, operating from 0.8 to 2.4 GHz, demonstrates measured drain efficiency in the ranges of 57%–78% under low compressions. In [11] a design for

*Corresponding author's email: sheikhi.a@lu.ac.ir

Table 1. Impedance Characteristics of Class-E/F, Class-J, and Class-E/FJ PAs.

PA Type	f_0	$2f_0$	$3f_0$
Class-E/F	*RLC*	Capacitive	Short
Class-J	(1+j)*R*	-j(3π/8)*R*	Open
Class-E/FJ	(1+j)*R*	Capacitive	Short

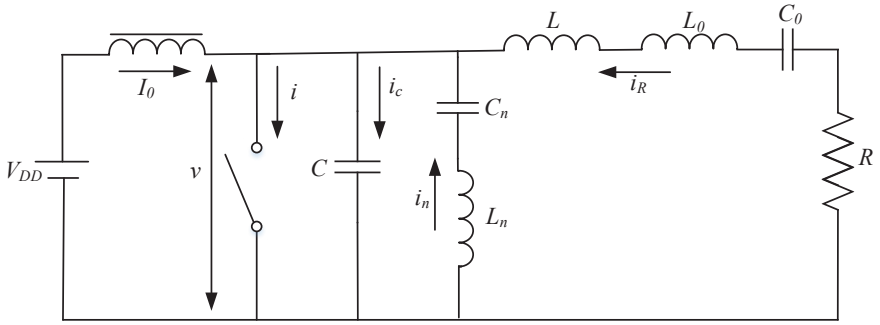

Fig. 1. The schematic of Class-E/F PA.

high-efficiency broadband class-B/J PA using active second harmonic injection is presented. The technique optimizes phase shift for improved efficiency and power. The PA was fabricated and tested from 1.1 to 1.7 GHz with an average efficiency of 74.4%.

This paper introduces an innovative hybrid Class-E/FJ PA that integrates elements of both Class-E/F and Class-J designs to achieve sustained high efficiency and broad bandwidth. The analysis, using the CGH40010F transistor model, delves into impedance characteristics in traditional Class-E/F and Class-J power amplifiers. Through a comprehensive examination, the study identifies specific design conditions tailored to the unique characteristics of Class-E/FJ PA.

2- Analysis of The PAs

The table provides information on the harmonic termination characteristics of various power amplifier types, including Class-E/F, Class-J, and Class-/FJ PA. As indicated in Table 1, the impedance harmonic termination of the Class-E/FJ PA is noteworthy. At the fundamental frequency, it exhibits a characteristic impedance of (1+j)*R*. Notably, at the second harmonic, the impedance behaves like a capacitor, while at the third harmonic, the impedance characteristic transforms into a short circuit. A hybrid Class-E/FJ amplifier is aimed to be reached by analyzing both Class-E/F and Class-J PAs. Subsequently, the conditions for transitioning to the Class-E state are analyzed.

Top of Form

2- 1- Analysis of Class-E/F PA

Fig. 1 illustrates the schematic diagram of the traditional hybrid Class-E/F PA. This configuration comprises both Class-E and Class-F^{-1} PAs. The expression for the optimal fundamental load impedance, referred to as Z_{opt}, in a Class-E/F PA is provided as part of the system description.

$$Z_{opt} = \frac{R}{1+\omega^2 R^2 C^2} + j[\omega L - \frac{R^2 \omega C}{1+\omega^2 R^2 C^2}] \quad (1)$$

The current through the shunt capacitance produces the switch voltage. The switch-voltage waveform satisfies the zero voltage switching (ZVS) and zero voltage derivative switching (ZVDS) conditions at the switch turn-on instant. It is assumed that the switch for an interval of $0 \le \theta \le 2\pi D$ is

ON. D is a duty cycle.

The ZVS and ZVDS conditions required for Class-E/F PAs are expressed as:

$$v(\omega t)\big|_{\omega t=2\pi D} = 0 \tag{2}$$

$$\frac{dv(\omega t)}{d\omega t}\big|_{\omega t=2\pi D} = 0 \tag{3}$$

Where $v(\omega t)$ is the voltage of the switch. For the simplified circuit diagram of a Class-E/F PA presented in Fig. 1, when the switch is turned on for $0 \le \theta \le 2\pi D$ the correlation between currents can be articulated as:

$$i(\omega t) = I_0 + I_n sin\ n\omega t + I_R sin(\omega t + \phi) \tag{4}$$

I_0 is the DC supply current. The load current i_R is assumed sinusoidal as:

$$i_R(\omega t) = I_R sin(\omega t + \phi) \tag{5}$$

Where ϕ is the initial phase and I_R is the amplitude. The switch current can be written as:

$$i_n(\omega t) = I_n \sin(n\omega t) \tag{6}$$

Where I_n represents the amplitude of the nth harmonic current, and under the initial on-state condition ($i(0) = 0$), Eq. (4) can be expressed as follows:

$$I_0 + I_R sin\ \phi = 0 \rightarrow \frac{I_R}{I_0} = \frac{-1}{sin\ \phi} \tag{7}$$

When the switch is turned off in the range $2\pi D \le \theta \le 2\pi$, there is no current flowing through the switch, denoted as $i(\omega t) = 0$, while the current flowing through capacitor C can be represented as:

$$i_C(\omega t) = I_0 + I_n sin\ n\omega t + I_R sin(\omega t + \phi) \tag{8}$$

The voltage across the switch that occurs as a result of the capacitor charging can be obtained as:

$$\begin{aligned} v(\omega t) &= \int_{2\pi D}^{\omega t} i_C(\omega t)\, d\omega t \\ &= \frac{1}{\omega C}\left\{ \begin{array}{l} I_0(\omega t - 2\pi D) - \frac{I_n}{n}\left(cos(n\omega t) - cos 2\pi nD\right) \\ -I_R\left(cos(\omega t + \phi) - cos(2\pi D + \phi)\right) \end{array} \right\} \end{aligned} \tag{9}$$

Enforcing a zero-voltage switching condition in Eq. (2) on Eq. (9) yields:

$$\begin{aligned} &\frac{1}{\omega C}\left[(2\pi - 2\pi D) I_0 - \frac{I_n}{n}\left(\cos 2\pi n - cos\, 2\pi nD\right)\right. \\ &\left. -I_R\left(cos\,(2\pi + \phi) - cos\,(2\pi D + \phi)\right)\right] = 0 \end{aligned} \tag{10}$$

After simplifying Eq. (10):

$$\begin{aligned} &2\pi(1 - D) + \frac{I_n}{n}\left(cos\, 2\pi nD - 1\right) \\ &+ \frac{I_R}{I_0}\left(cos\,(2\pi D + \phi) - cos\ \phi\right) = 0 \end{aligned} \tag{11}$$

Applying a Fourier series expansion to Eq. (4) allows the determination of the relative amplitude of the nth harmonic component I_n/I_0 for any n

$$\begin{aligned} &\frac{1}{\pi}\int_0^{2\pi D} I_0\ sin\ n\omega t d\omega t \\ &+ \frac{1}{\pi}\int_0^{2\pi D} I_0\ sin^2 n\omega t d\omega t = 0 \end{aligned} \tag{12}$$

Consequently, the relative amplitude of the nth harmonic component I_n/I_0 can be obtained as:

$$\frac{I_n}{I_0} = \frac{4\left(1 - cos 2\pi nD\right)}{4n\pi D - sin 4n\pi D} \tag{13}$$

Through the substitution of Eq. (7) and Eq. (13) into Eq. (11), one can explicitly determine the initial phase angle ϕ for any D:

$$\phi = tan^{-1}\left(\frac{cos\ 2\pi D\ - 1}{2\pi(1 - D) - \frac{4\left(1 - cos\ 2\pi nD\right)^2}{n\left(4n\pi D - sin\ 4n\pi D\right)} + sin\ 2\pi D} \right) \tag{14}$$

The determination of the DC supply voltage V_{DD} involves employing a Fourier series expansion on Eq. (9) as follows:

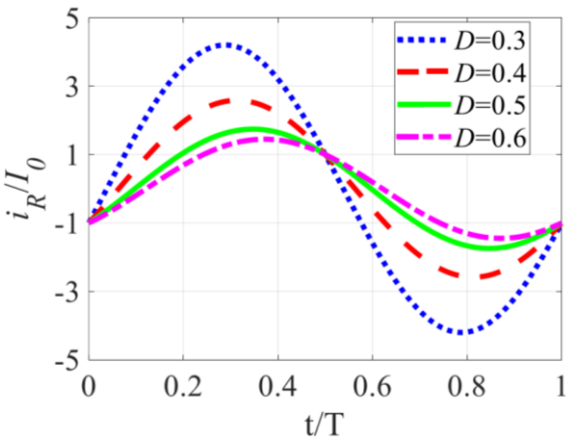

Fig. 2. The normalized resistor current waveform versus D for Class-E/F PA.

$$
\begin{aligned}
V_{DD} &= \frac{1}{2\pi}\int_{2\pi D}^{2\pi} v(\omega t)\,d(\omega t) = \\
&\frac{I_0}{2\pi\omega C}\left[\left(2\pi^2(D-1)^2\right)\right. \\
&-\frac{I_R}{I_0}(\sin\phi - \sin(2\pi D+\phi) \\
&-2\pi(1-D)\cos(2\pi D+\phi)) \\
&+\frac{I_n}{n^2 I_0}\sin(2\pi Dn) \\
&\left.+2\pi n(1-D)\left(\cos(2\pi nD)\right)\right]
\end{aligned}
\tag{15}
$$

With an idealized collector efficiency of 100%, the DC power $P_0 = I_0 V_{DD}$ and the fundamental-frequency output power $P_{out} = V^2_R/2R$ delivered to the load are equivalent. where $V_R = RI_R$. Utilizing Fourier formulas and Eq. (9), the amplitudes of these components can be determined.

$$
\begin{aligned}
V_R &= \frac{-1}{\pi}\int_{2\pi D}^{2\pi} v(\omega t)\sin(\omega t+\phi)\,d(\omega t) = \\
&-\frac{I_0}{\pi\omega C}\left[(2\pi D-2\pi)\cos\phi\right. \\
&+\left(\sin\phi - \sin(2\pi D+\phi)\right) \\
&-\frac{I_R}{I_0}\left(\frac{\cos(4\pi D+2\phi)-\cos 2\phi}{4}\right. \\
&+\cos\phi\cos(2\pi D+\phi)-\cos^2(2\pi D+\phi)) \\
&-\frac{I_n}{nI_0}\left(\frac{\cos(2\pi D(n+1)+\phi)-\cos\phi}{2(n+1)}\right. \\
&+\frac{\cos(2\pi D(1-n)+\phi)-\cos\phi}{2(1-n)} \\
&\left.-\cos 2n\pi D(\cos(2\pi D+\phi)-\cos\phi))\right]
\end{aligned}
\tag{16}
$$

$$
\begin{aligned}
V_L &= \frac{-1}{\pi}\int_{2\pi D}^{2\pi} v(\omega t)\cos(\omega t+\phi)\,d(\omega t) = \\
&-\frac{I_0}{\pi\omega C}\left[\left(\cos\phi - \cos(2\pi D+\phi)+2\pi(1-D)\sin\phi\right)\right. \\
&-\frac{I_R}{I_0}\left(\pi(1-D)+\frac{\sin(2\phi)-\sin(2\phi+4\pi D)}{4}\right. \\
&-\sin\phi\cos(2\pi D+\phi)+\frac{\sin(2\phi+4\pi D)}{2}) \\
&-\frac{I_n}{nI_0}\left(\frac{\sin\phi-\sin(2\pi D(n+1)+\phi)}{2(n+1)}\right. \\
&-\frac{\sin\phi-\sin(2\pi D(n\text{-}1)+\phi)}{2(n-1)} \\
&\left.\left.-\cos(2\pi Dn)(\sin\phi-\sin(\phi+2\pi D))\right)\right]
\end{aligned}
\tag{17}
$$

Fig. 2 displays the normalized resistor current as a function of the D parameter. From Fig. 2, it is clearly shown that the peak normalized resistor current is decreased as the value of D is increased.

Figs. 3 and 4 further depict the normalized switch current and voltage waveforms, respectively, for various values of the D parameter. It is evident that, with an increase in D, the normalized amplitude of the switch current decreases, while the normalized amplitude of the switch voltage increases. The normalized resistance is obtained based on the output power definition ($P_{out}=V_R^2/2R$) and Eq. (7).

$$
\frac{RP_{out}}{V_{DD}^2} = 2\left(\frac{I_0}{I_R}\right)^2 = 2\sin^2\varphi \tag{18}
$$

The output power denoted as P_{out}, is a key metric.

In Fig. 5, it is depicted that the normalized resistance (RP_{out}/V_{DD}^2) increases with a rise in D. Therefore, according

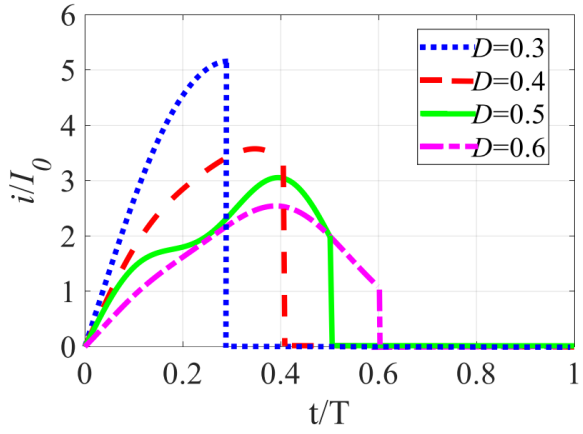

Fig. 3. The normalized switch current waveform versus D for Class-E/F PA.

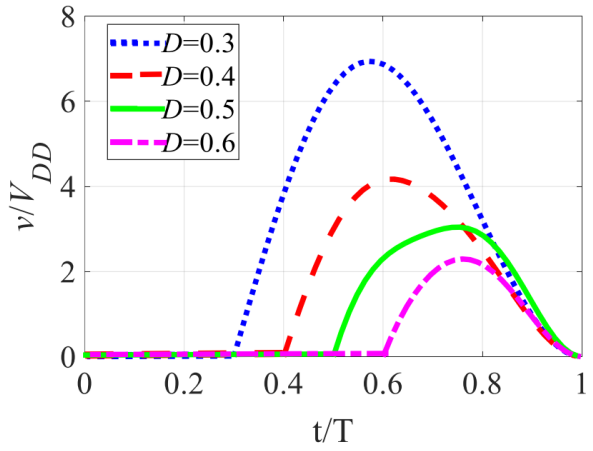

Fig. 4. The normalized switch voltage waveform versus D for Class-E/F PA.

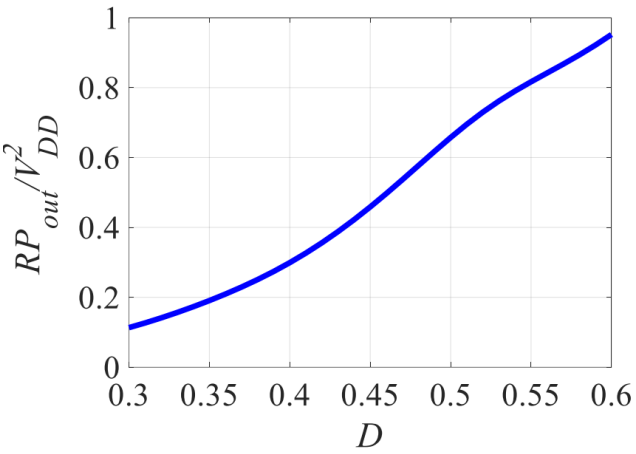

Fig. 5. The normalized resistance (RPout/VDD2) versus D for Class-E/F PA.

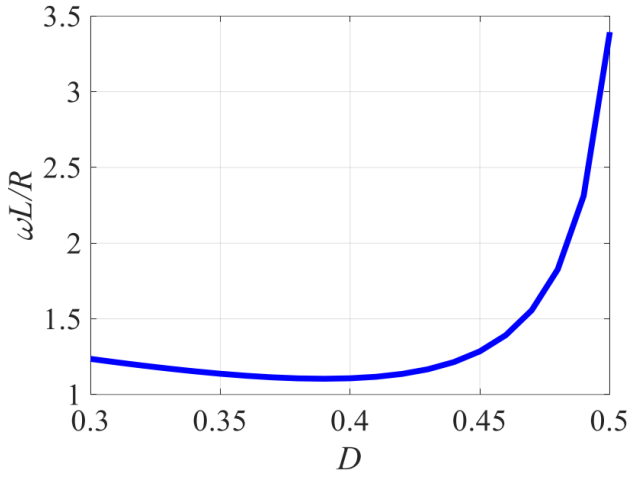

Fig. 6. The (ωL/R) waveform of Class-E/F PA versus D.

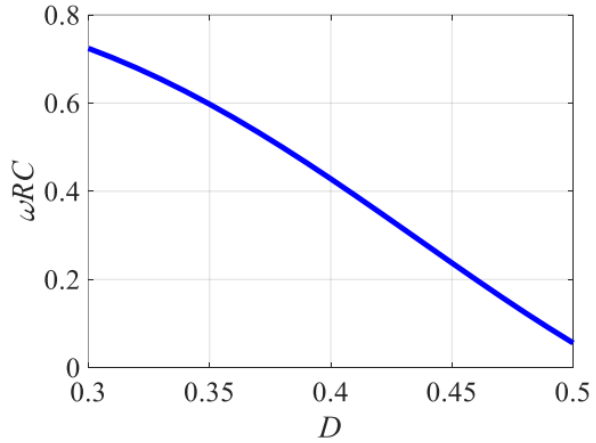

Fig. 7. The (ωRC) waveform of Class-E/F PA versus D.

to the schematic of the Class-E/F amplifier in Fig.1, the optimal values for normalized series inductance (L) can be determined through the following calculation.

$$\frac{\omega L}{R}=\frac{V_L}{V_R} \tag{19}$$

Fig. 6 illustrates the $\omega L/R$ for various values of D. It is evident from the graph that the magnitude of $\omega L/R$ decreases until $D = 0.4$. After reaching $D = 0.4$, the waveform of $\omega L/R$ exhibits an upward trend. According to Eqs. (7) and (16), the optimum value of shunt capacitance (C) can be determined from:

$$\omega RC=\frac{\omega CV_R}{I_0}\times\frac{I_0}{I_R} \tag{20}$$

Fig. 7 illustrates the variation of ωRC concerning D. It is evident that as the duty cycle increases, the value of ωRC decreases. Typically, both Class-E and inverse Class-F amplifiers are designed to operate within a specific frequency or a narrow frequency band. The output networks in these classes are often tuned to maximize efficiency and performance at a particular frequency. Although the

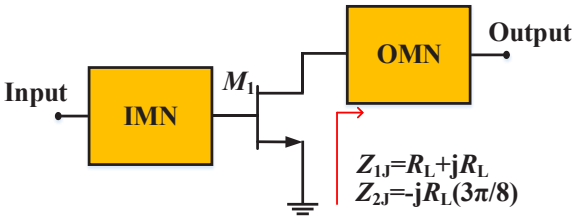

Fig. 8. The general topology of Class-J PA.

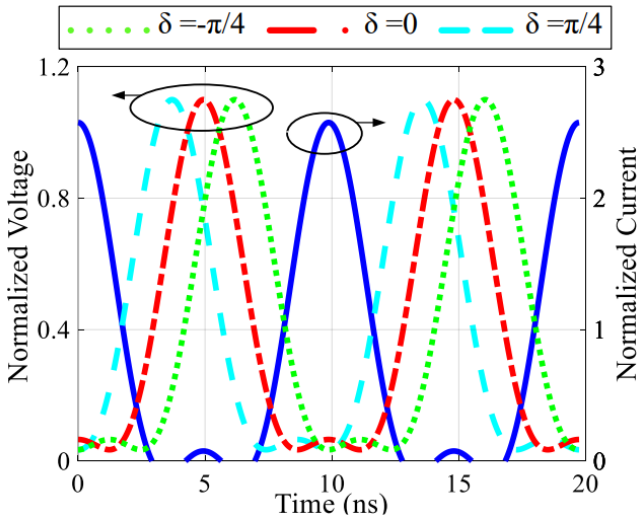

Fig. 9. The voltage and current waveforms of Class-J PA.

bandwidth of Class-E/F amplifiers may be relatively limited compared to certain other amplifier classes, it is essential to highlight that Class-E/F PA is purposefully designed with a primary emphasis on achieving high efficiency.

2- 2- Analysis of Class-J PA

Fig. 8 illustrates the general topology of a Class-J PA. The transistor's gate and drain bias voltages are supplied through the input matching network (IMN) and output matching network (OMN), respectively.

The IMN facilitates impedance matching between the input RF port and the input impedance of M_1, while the OMN provides the necessary impedance for optimal operation of M_1 at fundamental frequency and second harmonic. Similar to its Class-B counterpart, a Class-J PA is biased, and its drain-source current follows a half-sinusoidal waveform, as expressed by:

$$i_{DS}(\theta)=\frac{I_{max}}{\pi}+\frac{I_{max}}{2}\cos(\theta)+\frac{2I_{max}}{3\pi}\cos(2\theta)+\ldots \qquad (21)$$

where I_{max} is the maximum current of the transistor, and $\theta=\omega_0 t$ represents the angular phase.

In its simplest form, a Class-J PA is a second-harmonic tuned PA and $v_{DS}(\theta)$ is given by

$$v_{DS}(\theta)=V_{DD}-(V_{DD}-V_K)\times \left[\sqrt{2}\cos(\theta-\delta)-0.5\cos(2\theta-2\delta)\right] \qquad (22)$$

where V_K is the knee voltage of the transistor, and δ is the phase difference between v_{DS} and i_{DS} from 180◦.

Fig. 9 displays the voltage and current waveforms of a Class-J PA as determined by theoretical equations. The degree of overlap between these waveforms is determined by the parameter δ. In an ideal Class-J PA, the value of δ corresponds to $\pi/4$. According to the theory of Class-J PAs, the load impedance of Class-J PA can be obtained as follows:

$$Z_1 = \frac{(V_{DD}\text{-}V_K)(1+j)}{I_{max}/2} = (1+j)R_L \quad (23)$$

$$Z_2 = \frac{-(V_{DD}\text{-}V_K)(j)}{2I_{max}/3\pi} = -j\frac{3\pi}{8}R_L \quad (24)$$

The ideal load resistance (R_L) can be determined through the following calculation:

$$R_L = \frac{2V_{DD}}{I_{max}} \quad (25)$$

Hence, for a CGH40010F transistor model V_{DD}=28 V, and a maximum drain current of 1.5 A, the ideal load resistance (R_L) should be approximately 37.33 Ω.

2- 3- Analysis of Class-E/FJ PA

The Class-J PA offers a versatile design space, allowing for efficient output power at both the fundamental impedance and second harmonic. This characteristic renders the amplifier well-suited for broadband and multiband applications. Consequently, the combination of two amplifiers—Class-E/F and Class-J—can prove highly practical in achieving a hybrid PA that embodies both high efficiency and a broad bandwidth. To realize the operational conditions of a Class-J amplifier and seamlessly integrate it with a Class-E/F amplifier, the Class-E/F conditions should be tailored to achieve a resistance value of 37.33 Ω. Therefore, the design of a PA should align with the Class-E/F conditions, approaching the characteristics from Class-E/F to Class-J. In the case of a Class-E/F PA, achieving 100% efficiency implies that the DC power matches the output power. Then the output power can be obtained as:

$$I_0 V_{DD} = \frac{RI_R^2}{2} \quad (26)$$

The real part of the optimal fundamental load impedance according to Eqs. (7), and Eq. (24), can be calculated as

$$R = \frac{2P_{out}}{I_R^2} = 2\sin^2\varphi\frac{P_{out}}{I_0^2} \quad (27)$$

For 10W output power, to achieve R = 37.33Ω, the parameter values of ϕ = −28.03, I_R/I_0 = 2.12, I_n/I_0 = 0.06 and D= 0.46 have been selected. Therefore, D should be set to 0.46 for the Class-E/F PA. At this juncture, it becomes evident that traditional Class-E/F PAs and conventional Class-J PAs can be effectively combined when specific conditions are satisfied. This paper focuses on harmonics up to the third order. To simplify circuit design, the harmonic impedances of the Class-E/F PAs are defined as follows:

$$Z_{2f_0|E/F} = \frac{1}{j\omega C} \quad (28)$$

$$Z_{3f_0|E/F} = 0 \quad (29)$$

For the proposed Class-E/FJ PA, the fundamental impedance is obtained as follows:

$$Z_{f_0|E/FJ} = (1+j)R^* \quad (30)$$

Also, the harmonic impedances of the Class-E/FJ PAs are defined as follows:

$$Z_{2f_0|E/FJ} = \frac{1}{j\omega C^*} \quad (31)$$

$$Z_{3f_0|E/FJ} = 0 \quad (32)$$

where R* and C* according to Eqs. (21), (22), and (23) for the proposed Class-E/FJ PA are 37.33 Ω and 1.7 pF, respectively.

3- Simulation and Measurement Results

To assess the performance of the proposed PA, a broadband high-efficiency PA is designed using CGH40010F GaN HEMT on Rogers 4003C substrate (ϵ = 3.55, h = 0.508mm). The drain DC bias voltage is set at 28 V, while the gate voltage is adjusted to −2.7V. To ensure the proposed PA meets the impedance requirements, impedance matching and harmonic control circuits are meticulously designed. In Fig. 10, the harmonic control circuits are illustrated, considering the transistor package parameters to ensure design accuracy. The trajectory of the OMN for the PA is determined using the large signal model. Subsequently, the impedance trajectory of fundamental, second, and third harmonics at the package plane and the I-Gen plane are observed and depicted in Fig. 11 (a) and (b). These circuits are vital for achieving optimal performance and efficiency in the PA design.

The schematic of the proposed Class-E/FJ PA is depicted in Fig. 12, while the implemented PA is shown in Fig. 13. The Class-E/FJ PA is unconditionally stabilized through the incorporation of two series resistors (R_1 = 4.7Ω, R_2 = 100Ω), utilizing ATC700A Series NPO Porcelain and Ceramic Multilayer Capacitors, along with mesa resistors bearing part number S0705CPX.

The IMN for the PA is designed to transform the optimum source impedance to 50Ω. Also, the simple OMN is employed to configure the conditions of the PA. The simulated voltage and current waveforms of the Class-E/FJ PA are plotted

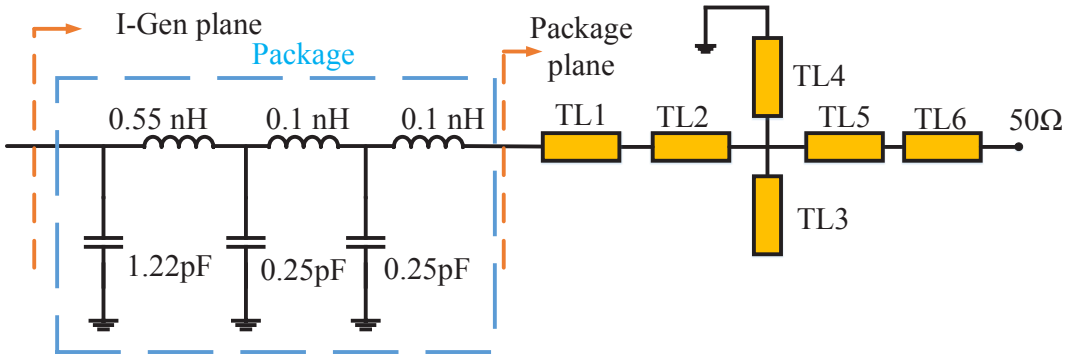

Fig. 10. Harmonic control circuit at the current generator plane.

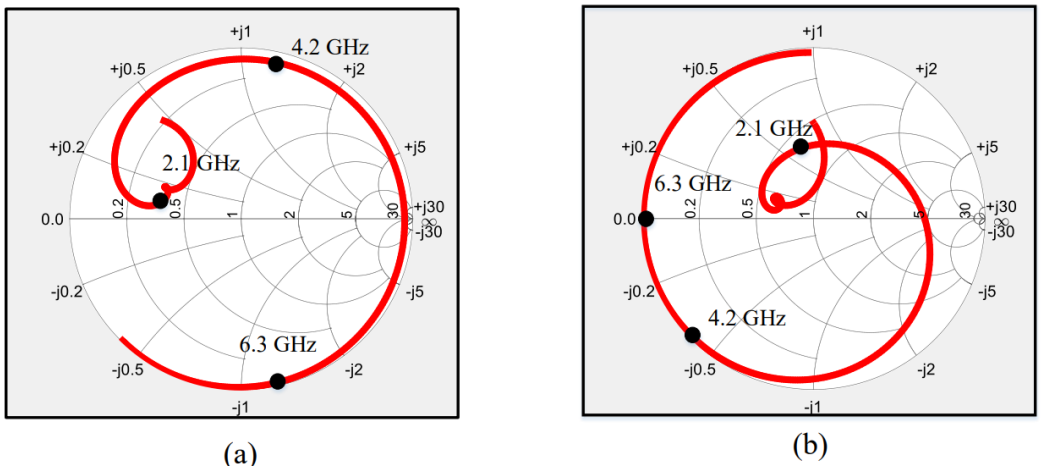

Fig. 11. Intrinsic impedance for the proposed Class-E/FJ PA (a) at the package plane (b) at the I-Gen plane.

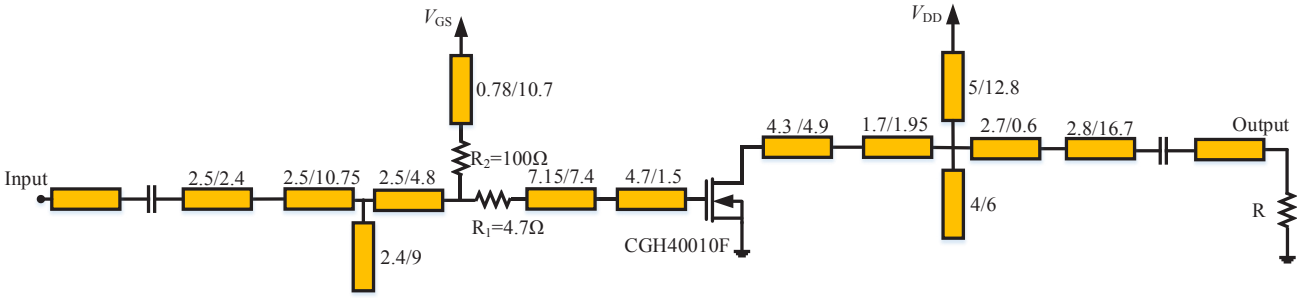

Fig. 12. Final schematic of the proposed Class-E/FJ PA.

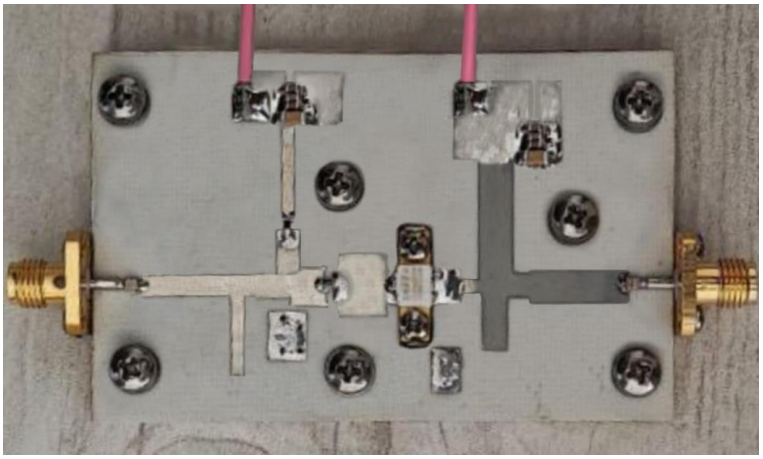

Fig. 13. Photograph of the proposed Class-E/FJ PA.

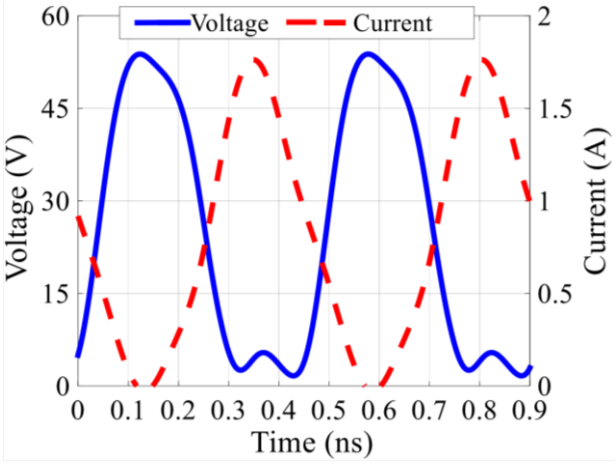

Fig. 14. The simulated waveforms of the proposed Class-E/FJ PA.

in Fig. 14. The waveforms illustrated in Fig. 14 serve as confirmation for the recommended operational class of the proposed amplifier.

A sensitivity analysis for the proposed PA simulated is shown in Fig. 15. Based on this study, the sensitivity of the amplifier's performance to different values of an R_1 resistor in the range of 1Ω to 18 Ω has been examined. This leads to selecting the optimal value for the resistor, considering the stability of the amplifier.

Fig. 16 shows the linearity performance of the amplifier in terms of third-order intermodulation products and intercept IP3. Intercept IP3 represents the point where the fundamental tone power equals the third-order product power if the amplifier behaves linearly. The simulation results in Fig. 16 indicate an impressive output intercept IP3 of around 43 dBm for the proposed PA, demonstrating excellent linearity.

Figs. 17(a), (b), and (c) illustrate how the Class-E/FJ PA performs at three different frequencies (1.3, 2.1, and 3.1 GHz). These figures depict the efficiency, PAE, and output power of the amplifier across the provided input power range. Fig. 17 demonstrates that the performance of the PA is favorable across all three given frequencies within its operational bandwidth range. Fig. 18 presents both simulation and measurement results for the proposed hybrid Class-E/FJ PA under continuous wave (CW) signals. The assessment spans from 1.3 to 3.1 GHz, revealing a notable achievement with a drain efficiency ranging from 63% to 73.4%. The feasible bandwidth of the designed PA extends from 1.3 to 3.1 GHz, demonstrating a substantial 55% bandwidth coverage. In Fig. 19, the performance of the Class-E/FJ PA is presented in

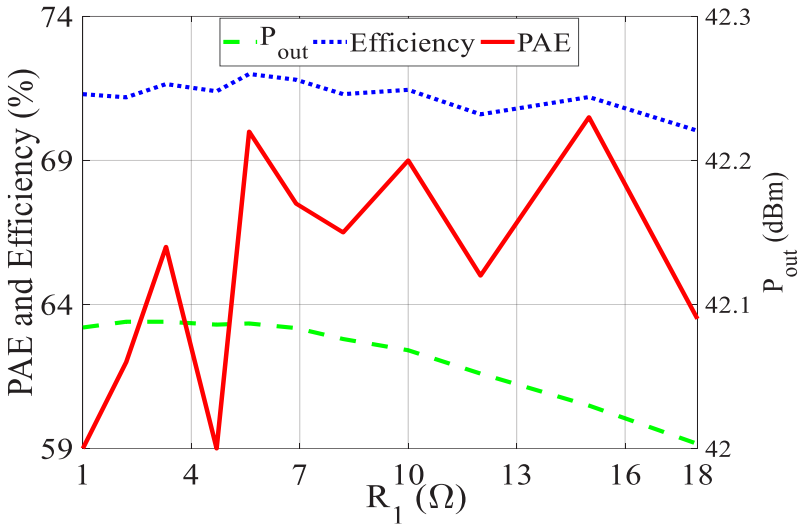

Fig. 15. The simulated sensitivity waveforms of proposed Class-E/FJ PA in terms of R1.

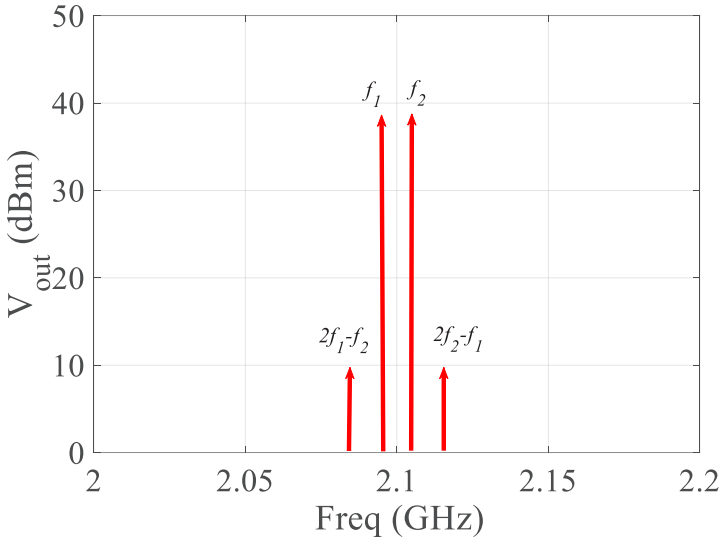

IP3_Lower	IP3_Upper
43.185	43.199

Fig. 16. The two-tone simulation of the proposed Class-E/FJ PA.

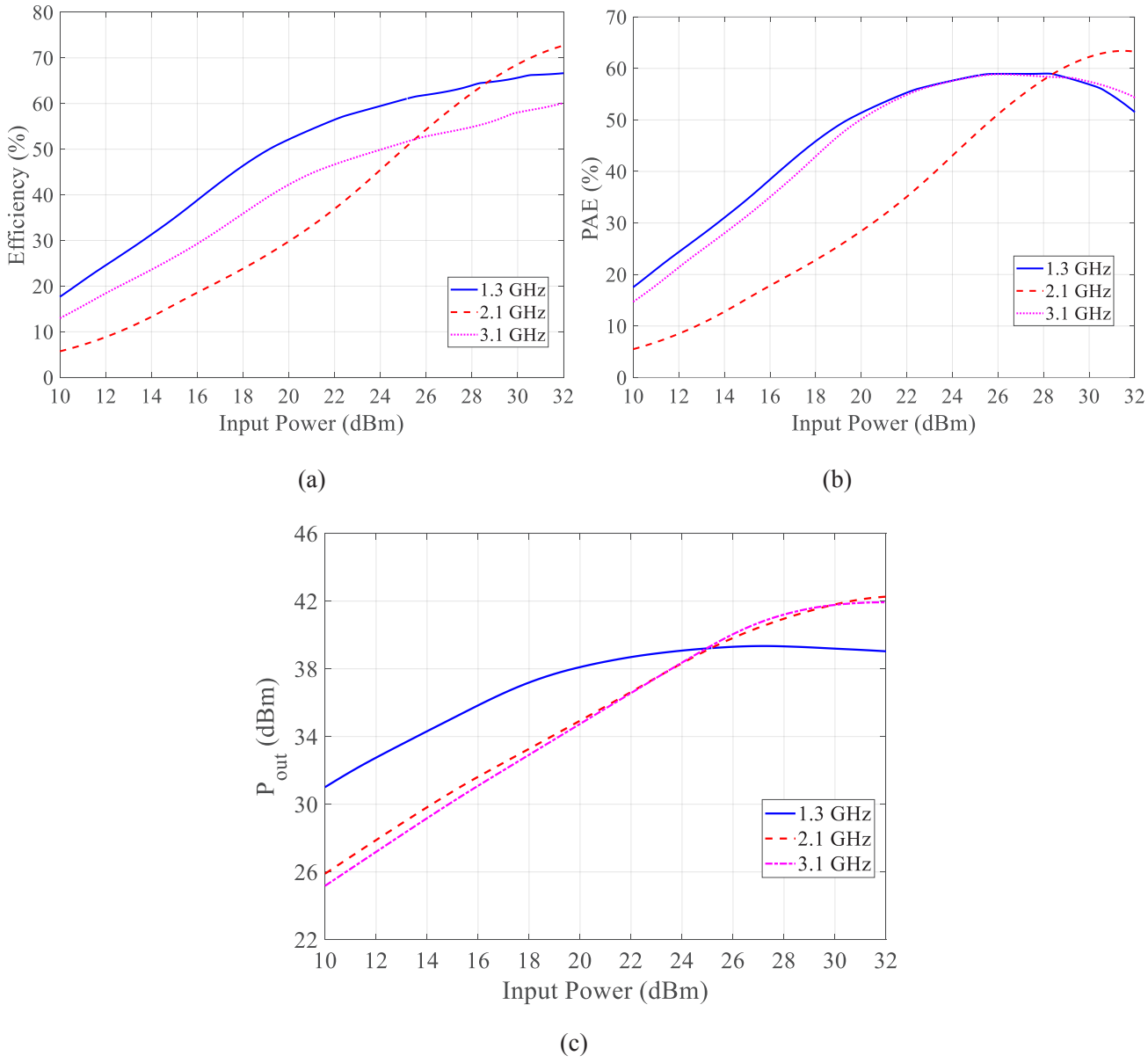

Fig. 17. The performance of the proposed PA versus input power in three different frequencies (a) efficiency, (b) PAE, and (c) output power.

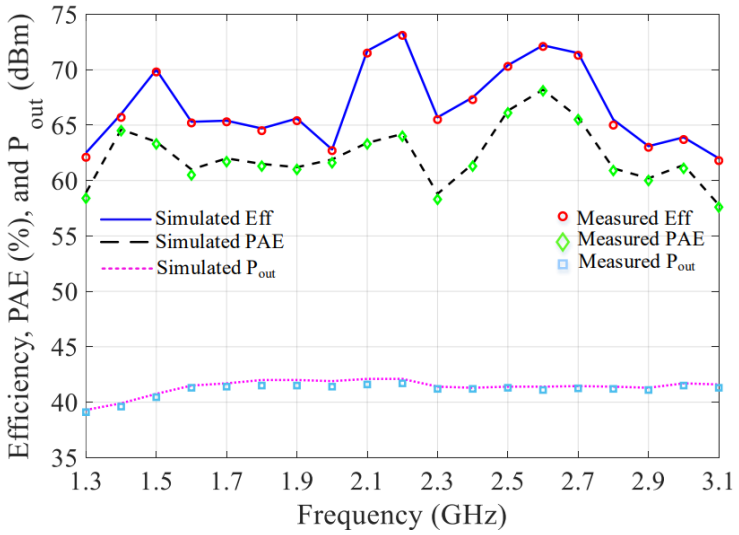

Fig. 18. Efficiency, PAE, and output power of the proposed PA versus frequency.

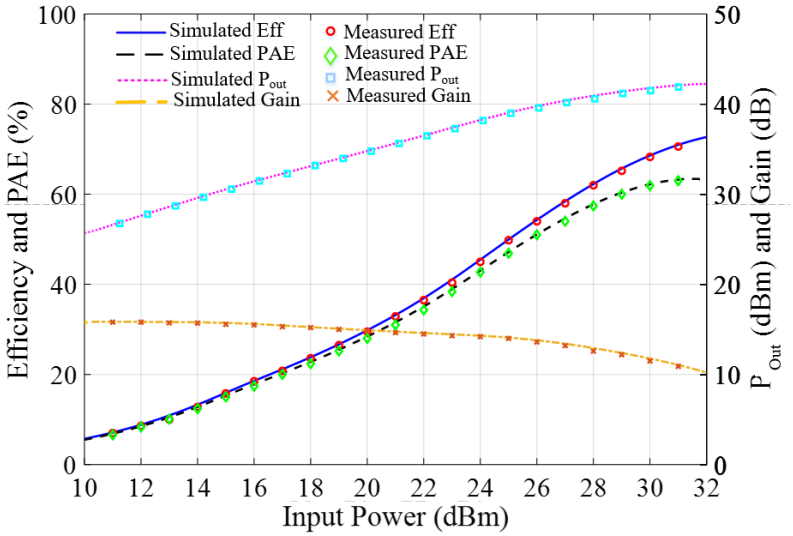

Fig. 19. Efficiency, PAE, gain, and output power of the proposed PA versus input power.

Table 2. Comparison between performances of this work with other previous PAs

Ref.	Class	f_0 (GHz)	Pout (dBm)	DE (%)	PAE (%)
[12]	E	1.4-2.7	39.7-41.5	63-73	-
[13]	CF	1.5-2.5	39.5-41.46	61-73.5	55-72
[14]	F	2.5-2.7	40.9-42.1	66.3-71.1	-
[15]	EF	2.6-3.6	40.7-41.6	62-78	-
[16]	EF	1.6-2.6	40.4-41.3	67-72	-
[17]	EF	2.5-3.6	39.5-41.2	69.5-79.2	-
[18]	J	1.4-2.6	39.5-40	60-70	50-60
[19]	J	1-4-2.4	39.8-40.3	63-68.9	58-64.9
This work	E/FJ	1.3-3.1	39.3-42.1	61.5-73.4	58.9-67.6

terms of input power at a frequency of 2.1 GHz. At the center frequency, the amplifier exhibits an efficiency of 71.7%, a PAE of 63.4%, and achieves a gain exceeding 10dB, along with an output power of 42 dBm. The measured data aligns well with the simulated results, indicating a robust correlation between predicted and actual performance.

Table 2 presents a performance comparison of several related PAs. Notably, the proposed PA stands out with a significantly broader bandwidth than the other PAs. Additionally, in terms of drain efficiency, the proposed PA surpasses all other works. In summary, the Class-E/FJ PA design strikes a commendable balance between drain efficiency and bandwidth, making it a promising choice in this context.

4- Conclusion

This paper introduces a novel high-efficiency broadband Class-E/FJ PA. By scrutinizing the impedances of traditional Class-J and Class-E/F PAs, common features are identified. The performance of Class-J and Class-E/F PAs suggests that under specific conditions, these classes of PAs can be effectively combined. The proposed fabricated PA achieves a bandwidth of 1.3–3.1 GHz, delivering 10W output power, exceeding 10dB gain, and showcasing a remarkable 61.5%–73.4% drain efficiency across all frequency bands. Conducting a comparative analysis with similar predecessors, our proposed PA outshines its counterparts, demonstrating superior performance across a wide bandwidth. This study not only presents a groundbreaking hybrid Class-E/FJ PA but also contributes a comprehensive understanding of the underlying theoretical principles and a systematic design methodology for broadband PAs.

References

[1] M. Hayati, A. Sheikhi, A. Grebennikov, Class-F power amplifier with high power added efficiency using bowtie-shaped harmonic control circuit, IEEE Microwave and Wireless Components Letters, 25(2) (2015) 133-135.

[2] M.G. Sadeque, Z. Yusoff, S.J. Hashim, A.S.M. Marzuki, J. Lees, D. FitzPatrick, Design of wideband continuous class-F power amplifier using low pass matching technique and harmonic tuning network, IEEE Access, 10 (2022) 92571-92582.

[3] Y. Shen, J. Xu, J. Yi, E. Chen, V. Chen, Class-E power amplifiers incorporating fingerprint augmentation with combinatorial security primitives for machine-learning-based authentication in 65 nm CMOS, IEEE Transactions on Circuits and Systems I: Regular Papers, 69(5) (2022) 1896-1909.

[4] A. Sheikhi, H. Hemesi, Analysis and design of the novel class-F/E power amplifier with series output filter, IEEE Transactions on Circuits and Systems II: Express Briefs, 69(3) (2021) 779-783.

[5] A. Sheikhi, M. Thian, H. Hemesi, Optimum and Suboptimum Operations of Class-E/F3 Power Amplifier with Nonlinear Shunt Capacitance at Different Grading Coefficient, Circuits, Systems, and Signal Processing, 41(7) (2022) 3657-3678.

[6] S. Pezeshkpour, M.M. Ahmadi, Design Procedure for a High-Efficiency Class-E/F 3 Power Amplifier, IEEE Transactions on Power Electronics, (2023).

[7] W. Feng, W. Wu, X.Y. Zhou, W. Che, Y. Shi, Broadband high-efficiency quasi-class-J power amplifier based on nonlinear output capacitance effect, IEEE Transactions

on Circuits and Systems II: Express Briefs, 69(4) (2022) 2091-2095.

[8] A. Alizadeh, A. Medi, A broadband integrated class-J power amplifier in GaAs pHEMT technology, IEEE Transactions on Microwave Theory and Techniques, 64(6) (2016) 1822-1830.

[9] R. Amirpour, R. Darraji, F. Ghannouchi, R. Quay, Enhancement of the broadband efficiency of a class-J power amplifier with varactor-based dynamic load modulation, IEEE Microwave and Wireless Components Letters, 27(2) (2017) 180-182.

[10] H.-C. Chang, P. Roblin, Y. Hahn, J.I. Martinez-Lopez, C. Liang, K. Rawat, Frequency-agile class-J power amplifier with clockwise fundamental-and second-harmonic loads, IEEE Transactions on Microwave Theory and Techniques, 68(7) (2020) 3184-3196.

[11] C. Liu, F.M. Ghannouchi, Theory and Design of High-Efficiency Broadband Class-B/J Power Amplifiers With Active Second Harmonic Injection, IEEE Transactions on Microwave Theory and Techniques, (2023).

[12] A. Grebennikov, High-efficiency class-E power amplifier with shunt capacitance and shunt filter, IEEE Transactions on Circuits and Systems I: Regular Papers, 63(1) (2016) 12-22.

[13] E. Aggrawal, K. Rawat, P. Roblin, Investigating continuous class-F power amplifier using nonlinear embedding model, IEEE Microwave and wireless components letters, 27(6) (2017) 593-595.

[14] W. Huang, J. Liu, High-efficiency class-F power amplifier based on double spiral defected ground structure, International Journal of Electronics, 111(3) (2024) 485-498.

[15] Z. Zhang, Z. Cheng, G. Liu, Design of broadband Class EF power amplifier based on low-pass filter matching structure, IEICE Electronics Express, 16(12) (2019) 20190264-20190264.

[16] Z. Zhang, Z. Cheng, H. Ke, G. Liu, H. Sun, S. Gao, Design of broadband hybrid class EF power amplifier based on novel capacitance compensation structure, Microwave, and Optical Technology Letters, 62(3) (2020) 1069-1076.

[17] X. Wei, Y. Luo, A continuous Class-EF power amplifier based on the general continuous mode design theory, International Journal of Circuit Theory and Applications, 51(11) (2023) 5038-5049.

[18] P. Wright, J. Lees, J. Benedikt, P.J. Tasker, S.C. Cripps, A methodology for realizing high-efficiency class-J in a linear and broadband PA, IEEE Transactions on Microwave Theory and Techniques, 57(12) (2009) 3196-3204.

[19] C. Liu, Q.F. Cheng, Highly efficient broadband class-J power amplifier using modified multisection quarter-wave lines and short-circuited stubs, IET Microwaves, Antennas & Propagation, 13(11) (2019) 1860-1865.

HOW TO CITE THIS ARTICLE

P. Rostami, A. Sheikhi. Analysis and Design of a Novel Broadband and High-Efficiency Class-E/FJ Power Amplifier. AUT J Electr Eng, 56(3) (2024) 361-376.

DOI: 10.22060/eej.2024.22902.5569